Geophysical and Remote Sensing Techniques for Evaluating Historical Stratigraphy and Assessing the Conservation Status of Defensive Structures Heritage: Preliminary Results from the Military Buildings at San Filippo Bastion, Cagliari, Italy

Luca Piroddi[1(✉)], Sergio Vincenzo Calcina[1], Donatella Rita Fiorino[1], Silvana Grillo[2], Antonio Trogu[1], and Giulio Vignoli[1,3]

[1] Department of Civil Engineering, Environmental Engineering and Architecture, DICAAR, UniCA, Cagliari, Italy
lucapiroddi@yahoo.it
[2] Department of Chemical and Geological Sciences, DSCG, UniCA, Cagliari, Italy
[3] Geological Survey of Denmark and Greenland GEUS, Aarhus, Denmark

Abstract. This paper describes the preliminary results of integrated non-destructive surveys for the diagnosis of the materials and for the analysis of the underground structures of an historical building. The studied structure was built in the center of Cagliari, Italy. A single channel 200 MHz Ground Penetrating Radar (GPR) survey was carried out in order to provide the 3D reconstruction of the buried structures localized under the floor level of two rooms of the structure. Two 3D models of the underground environments were derived from orthogonal radar profiles. In addition, active Infrared Thermography (IRT) and Multispectral Imaging techniques (MSI) were utilized to perform the non-invasive inspection of the conditions of the surface materials. IRT images were processed via the Principal Component Analysis (PCA) technique. The reflective patterns of the GPR maps allowed to locate several buried anomalies. IRT data and MSI images have provided a fundamental support to enhance discontinuities and defects of the investigated surfaces.

Keywords: Historical architecture · Ground Penetrating Radar · Active Infrared Thermography · Multispectral Imaging · Integrated diagnostic methods

1 Introduction

Nowadays, both geophysical methods and non-destructive techniques are considered essential tools for the analysis of the integrity status of valuable historical structures. The increasing interest towards the restoration and the rehabilitation of ancient structures and monumental buildings has encouraged the use of these techniques for the diagnosis of the materials properties and the identification of defects, degradation, past

© Springer Nature Switzerland AG 2020
O. Gervasi et al. (Eds.): ICCSA 2020, LNCS 12255, pp. 944–959, 2020.
https://doi.org/10.1007/978-3-030-58820-5_68

interventions and pre-existing underground structures [1]. Several geophysical techniques were utilized to explore buried and external structures, such as foundations of historical buildings [2], ancient bridges [3], underground water systems and aqueducts [4], archaeological remains [5–8] and military architectures [9]. Geophysical surveys were performed to study the experimental dynamic behavior of historical structures [10–13] and ancient artificial urban caves [14]. Over the time, even miniaturized systems, so-called micro-geophysical methods, were improved to characterize construction materials, ancient walls, frescoes and historical artworks [15–18].

In this framework, the preliminary results of the integrated non-invasive surveys carried out within a monumental structure in the historical center of Cagliari (southern Sardinia, Italy) are discussed. Ground Penetrating Radar (GPR) surveys, Infrared Thermography (IRT) and Multispectral (MS) measurements have been applied. The surveyed structure is the "*Bastione di San Filippo*", constructed by the Piedmont Corps Engineers in the early 1700s, as a defensive reinforcement to the northwest of the city. The research has preliminary investigated the historical stratifications, the metamorphoses and changes in the uses of the spaces of the Bastion, closely related to the life of the military facility and uses, including the Royal Bakery dating back to 1823. At present, the Bastion houses the military library and the Military Red Cross, and it is a listed building since 2014 (Fig. 1.a). The structure comprises several buildings, belonging from different chronological phases. The most interesting structures are the two rectangular vaulted rooms - once used as a casemate - and other connected internal environments (Fig. 1.b–1.c) [19, 20].

The study has been carried out within the General Agreement signed in September 2018 by the University of Cagliari and the Italian Ministry of Defence [21].

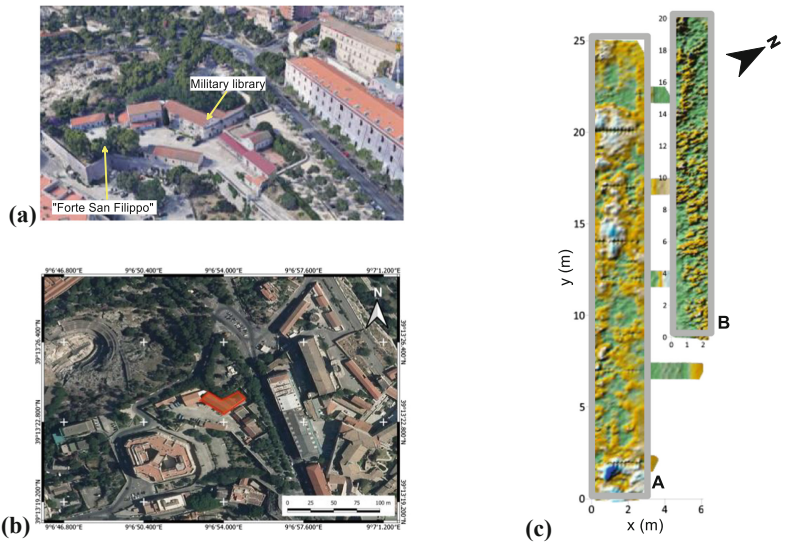

Fig. 1. Bastion of "*San Filippo*": (a) 3D image of the "*Forte San Filippo*" and the structure of the military library; (b) aerial image of the surveyed structure (red polygon); (c) schematic plan of the A and B rooms overlapped by the GPR maps. (Color figure online)

2 Materials and Methods

2.1 Ground Penetrating Radar: General Principles and Data Collection

GPR methods include different geophysical techniques based on the use of transmitted and/or reflected high-frequency microwave pulses. Generally, a transmitter generates the electromagnetic signals that, in turns, are collected by a receiving unit. The GPR techniques comprise different layouts of acquisition. In particular, transmitter and receiver can be separated (bistatic configuration) or can be the same antenna (monostatic configuration). The electromagnetic (EM) signals recorded at the receiver antenna permit to estimate both electrical and magnetic properties of the investigated materials. The velocity of the electromagnetic pulses travelling through materials with low-magnetic susceptibility depends on both the relative dielectric permettivity (ε_r) and the relative magnetic permittivity (μ_r) of the medium, according to the following equation [22]:

$$v = \frac{c}{\sqrt{\varepsilon_r \mu_r}} \tag{1}$$

The attenuation of the radar signals decreases as the frequency decreases (and/or when the electrical conductivity increases). Therefore, this parameter directly affects the depth of investigation of the GPR survey and both vertical and horizontal spatial resolution. It is possible to estimate the resolution of the radar survey starting from the wavelength of the electromagnetic signal. As a rule of thumb, the spatial resolution corresponds to about one-quarter of the wavelength of the signal.

The radar antenna is designed to transmit microwave signals over a specific bandwidth of frequencies with maximum power in correspondence to a central frequency. The spectral position of the maximum power peak of the transmitted waveform is inversely proportional to the duration of the radar pulse [20]. The bandwidth of the emitted signal is equal to the peak frequency of the amplitude monochromatic spectrum.

Ground Penetrating Radar survey was carried out using the IDS, Fast Wave DAD system controlled by K2 Fast Wave software, acquisition unit operating in monostatic configuration with a central frequency of 200 MHz. The GPR survey allowed the investigation of the rooms indicated with the letters A and B in Fig. 1.c, by covering, in a relative short time (five hours) an area of 120 m^2. The time of acquisition was set to 110 ns in order to investigate down to a theoretical depth of investigation of around 5 m. The survey consisted of parallel radar profiles with a line-spacing of 0.5 m along the x-direction (short side of the room, Fig. 1.c). Additional radar profiles were acquired along the perpendicular direction with the same spatial interval (y-direction of Fig. 1.c) in order to create a regular grid. The horizontal distance along each radar profile was measured through the use of spatial markers in correspondence to pre-established positions of the antenna. The frequency band of the radar probe was chosen to meet the best compromise between a significant depth of investigation and a suitable spatial resolution of the radar survey. The geometry of acquisition was designed in order to assure both a suitable spatial coverage and a significant lateral resolution.

The radar data were processed through Reflexw package (by Sandmeier®). The processing flow was composed of de-wow, move start time, background removal, gain, band pass, time-to-depth conversion. 3D reconstruction of the GPR anomalies was done via the analysis of the spatial coherence of the reflected and the diffracted signals in the depth interval between the floor surface and about 2.9 m depth. The three-dimensional reconstruction inferred from the radar data allowed imaging the spatial extension of the electromagnetic anomalies in both vertical and horizontal directions.

2.2 Infrared Thermography (IRT): General Principles and Data Collection

The Infrared Thermography (IRT) technique is a completely non-destructive methodology consisting of active and passive measurements of the infrared radiation emitted by the studied object. During the IRT data collection, a digital infrared camera is utilized to acquire the signals in the frequency band of the thermal-infrared, where the bodies at common environmental temperatures have the maximum of EM emission. From the acquired data, it is possible to obtain a reliable estimation of the main physical properties of the materials; in particular, both the thermal properties (e.g. conductivity, diffusivity, effusivity and specific heat) and spectral properties (emissivity, absorption, reflection and transmission coefficients) of the material can be assessed [23]. These physical properties are indirectly connected to medium characteristics such as porosity, superficial roughness and moisture. In turns, these inferred features of the medium can be very helpful in the assessment of the defects, degradation status and water content of the materials and potentially their spatial distributions.

The active IRT was carried out via a digital thermal camera (FLIR System AB model P30 PAL). The measurements were acquired indoor with three different points of view. Hence, the collected IRT data can be considered not affected significantly by the external weather conditions.

The *Principal Component Analysis* (PCA) was performed to process the infrared (IR) time-lapse thermal data. This procedure is a widely used linear projection technique which was implemented to map the original ($m\ x\ p$) matrix $\boldsymbol{A}$ into a second ($s\ x\ p$) matrix $\boldsymbol{A_p}$ characterized by $s < p$. Basically, the matrix $\boldsymbol{A}$ is projected on a new system of principal axis, according to the following general relationship:

$$\boldsymbol{A_p} = \boldsymbol{U^T A} \tag{2}$$

where the columns of the matrix $\boldsymbol{U}$ include the projection vectors that maximize the variance in the projected $\boldsymbol{A_p}$. Therefore, this numerical technique highlights the uncorrelated projected distributions included in the data. The principal axes correspond to orthogonal eigenvectors of the square scatter matrix $\boldsymbol{S}$ ($m \times m$). PCA is usually performed via the *Singular Value Decomposition* (SVD).

In particular, the scatter matrix can be derived as follows:

$$\boldsymbol{S} = \boldsymbol{UDU^T} = [\boldsymbol{U_s U_n}] \begin{bmatrix} \boldsymbol{D_s} & 0 \\ 0 & \boldsymbol{D_n} \end{bmatrix} [\boldsymbol{U_s U_n}]^{\boldsymbol{T}}, \tag{3}$$

where the matrix $\boldsymbol{U}$ represents the modal matrix, or the eigenvector matrix, and $\boldsymbol{D}$ is the diagonal matrix corresponding to the eigenvalues of the scatter matrix.

The PCA of the IR thermographic data is suitable to enhance the visibility of defects in thermal infrared data and to improve the interpretation of the experimental IR images [24]. In the present study, the PCA of the IR data was performed by using a MATLAB® tool.

In parallel to the PCA approach and aiming at a wider support to experimental data interpretation, time dependent IRT datasets were also processed with other statistical approaches - like the regression models - aiming at further detecting the main features in the data by compacting the dynamic behavior into few images [25–28].

2.3 Multispectral Analysis: Methodology and Acquisition

Multispectral remote sensing applied to cultural heritage targets includes a family of techniques which investigate the surface finishes by means of their responses to extremely high frequency electromagnetic waves. Depending on frequency ranges used for energizing and sensing the artifacts we can choose transmission or reflection experimental configurations, also depending on the thickness of investigated objects. In particular, reflectometry, in the bands ranging from ultraviolet to near-infrared, can be used to highlights finishes defects and can enhance readability of drawings and paintings (sometimes even evidencing drawings completely invisible to eyes) by overcoming the shielding of exterior paintings layers and dirt patinas [16, 29–34].

In order to perform the multispectral survey, a modified digital single-lens reflex (DSLR) camera (original model NIKON D750) was used after removing the internal visible region passband filter: Five narrow EM bands from ultraviolet (UV) to near-infrared (NIR) were separately acquired with different exposure setups [17, 31–34]. In fact, the three colors channels of the standard sensors in many digital cameras are sensitive to an EM spectrum wider than visible spectrum. This additional portion of the recorded spectrum is generally filtered out though a bandpass filter installed by default by the manufacturer. Removing this filter (or substituting it with alternative filters - impacting other frequency bands – which can be added even in the external optics bodies) allows the users to acquire images over other ranges compatible with the full spectrum of the recording sensor (Fig. 2). The camera setup parameters were remotely controlled with the commercial acquisition software package Nikon Camera Control Pro 2. To make more uniform the target lighting, artificial halogen lights were utilized, and the contribution of natural light was highly reduced as the data were collected indoor.

The external bandpass EM filters, mounted over the optics, were:

- an UV bandpass filtering configuration, with acquisition in the range 320–390 nm;
- a visible bandpass filter with a window in the range 390–700 nm, to record images at visible wavelengths;
- an IR high pass filter at 720 nm;
- an IR high pass filter at 850 nm;
- an IR high pass filter at 950 nm.



Fig. 2. Raw data example acquired within multispectral survey.

Multispectral images were processed with a Multi Images Stacking (MIS) algorithm [31–33]. The results enhanced low-visible details related to artifacts contents or connected to the conditions of the target. With this technique, photographic acquisitions are done with different and variable camera exposure set-up, obtaining one RGB raw image for each chosen exposure; the recorded raw images are converted to 16 bit grayscale images and stacked together to generate an image which maintains a high level of detail optimized from each exposure acquisition (Fig. 3). This procedure is repeated for each spectral family of acquisitions (each EM passband filter).



Fig. 3. Stacked images after the application of Multi Images Stacking (MIS) algorithm.

3 Results and Discussion

3.1 GPR Results

The results of the GPR survey show a relatively complex patterns of anomalies with different sizes and shapes in both the investigated rooms. From the horizontal slices at different depth in Fig. 4 and Fig. 5, it is possible to detect several high-amplitude signal reflections characterized by a significant spatial (both vertical and horizontal) coherence. The amplitude of the radar signals decreases as the depth increases. In particular, the slices regarding the location A are characterized by five intense GPR shallow anomalies. with horizontal sizes ranging between 1.5 m and 4.5 m. Despite a theoretical depth of around 5 m, the actual survey volume goes from 0 m to 2.9 m depth, under which the signal-to-noise ratio is too low. These anomalies can be classified accordingly to their three-dimensional shape, their intensity and shape. The GPR anomalies, indicated with the symbols A1, A2 and A3 (red rectangles), form one group. They are characterized by intense signals with significant spatial continuity. The horizontal extension of the A1 anomaly increases with depth and reaches its maximum at about 2.5 m. The A2 anomaly is detected at 20 m along the y-direction of the local reference system and covers a surface of about 6 m^2. The anomaly A3 has an area of about 2 m^2 at the surface and has its maximum horizontal extension between 1 m and 2 m. The nature of these highly reflective patterns is not clearly identified. However, the anomalies highlight the presence of a marked heterogeneity in the distribution of the electrical and the magnetic properties of the subsurface materials. The high-amplitude anomalies A1 and A2 could be generated by the presence of outcrops of the underground bedrock or by buried artificial structures related to the construction of the fortifications (in this respect, a preliminary hypothesis to be verified is that A1 and A3 might be buttress of a portion of one of the several successions of defense walls of the city).

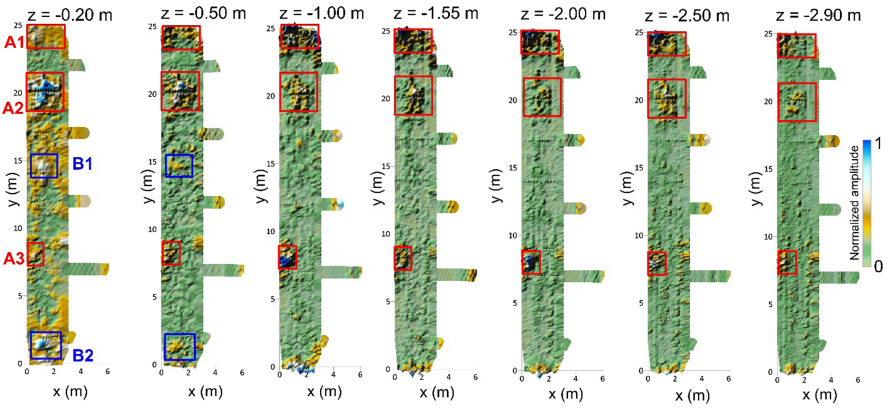

Fig. 4. GPR survey, room A: horizontal slices localized at a depth comprised between 0.2 m and 2.9 m. (Color figure online)

The geological units of the site mainly consist of limestone and superficial soils. Even other materials, used in the past to realize the embankment, can be locally observed. A second class of GPR anomalies includes relatively little reflective bodies, characterized by a smaller vertical extension; they are indicated with the letters B1 and B2 (blue rectangles) in Fig. 4. In particular, B2 shows its maximum amplitude at a depth between 0.1 and 0.5 m.

The GPR survey carried out in the room B highlights a more complex distribution of the electromagnetic signals. As we can see in Fig. 5, the pattern of anomalies is characterized by lower amplitude of the signals. The few detected anomalies of strong amplitude are localized in the depth interval: 0.5 to 1.5 m.

In particular, in the interval, in the y-direction, ranging from 15 m to 20 m, two GPR anomalies pop up. This set of anomalies are included inside the red rectangles indicated with the symbols D1 and D2 (but viseable also at z = –0.2 and z = –1.55). In the slices related to a depth of 0.20 m and 0.50 m two anomalies, indicated with the symbols C1 and C2, are visible. These bodies progressively vanish as depth increases. The GPR anomalies C3 and C4 appear at a depth of about 0.80 m from the surface of the pavement of the room B and reach a maximum vertical development equal to 1 m.

Based on the preliminary analysis, the nature of these reflective bodies is strongly uncertain and needs of further analyses. In this room, the GPR maps show also a higher frequency distribution of spatial features with minor amplitude, which can be interpreted as a higher noise level possibly masking significant anomalies or also as the EM response of preparatory works and rubbles accumulations for the hill profile flattening and pavement foundations.

However, the GPR results allow the identification of few interesting areas of significant amplitude to focus on during future investigations.

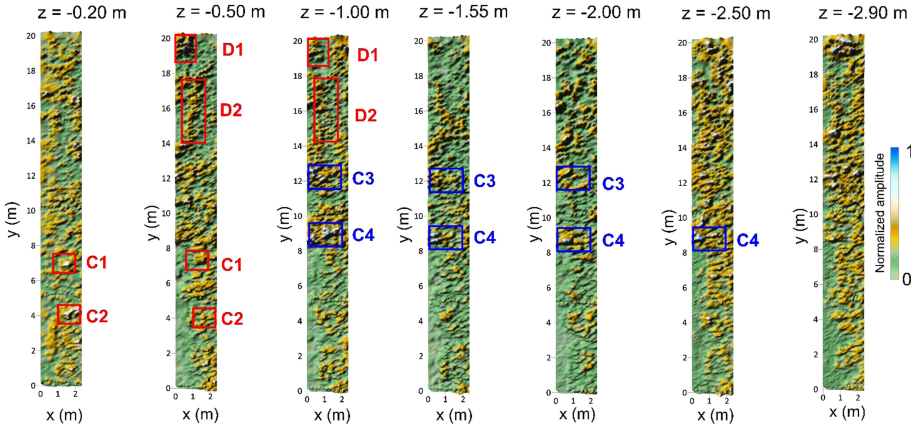

Fig. 5. GPR survey, room B: horizontal slices localized at depth comprised between 0.2 m and 2.9 m.

3.2 Description of IRT Results

The active IRT survey was performed to study the surfaces of the walls of the buildings in the study area. In particular, the investigation was performed to identify the main defects on the plasters of the internal walls, to assess the moisture content and patterns and other phenomena of degradation potentially correlated to different thermal properties of the construction materials. The images plotted in Fig. 6 show the IRT raw data.

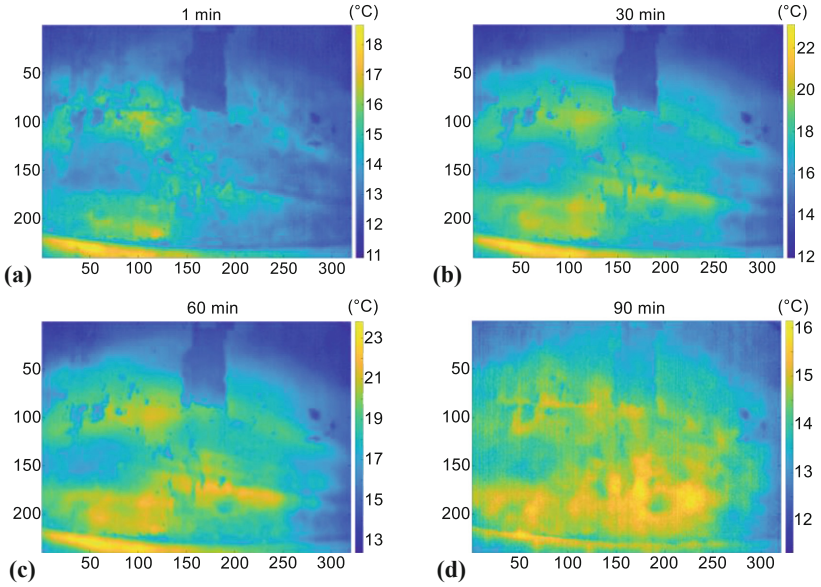

Fig. 6. Infrared Thermography: raw data acquired in correspondence to the position n.1, during heating and cooling phases. The color scale indicates the temperature of the surveyed surface. (Color figure online)

The preliminary analyses of the results highlight the presence of different thermal responses of the surveyed materials. These heterogeneous zones correspond to different stains with chromatic changes that could be attributed to the diffusion of biological colonization, dirt with varying moisture content and mold. Localized cracks, detachments and zones with loose adherence of the construction materials could be identified through the IRT inspection. The zones with loose adhesion of mortar usually result in higher temperatures due to the air filling the space between the wall and the detached surface thermally isolating the shallow layers from the deeper portions of the medium [35]. Thermal anomalies clearly show that the physicals properties of the materials are highly depending on the state of integrity. The warmer anomalies in the thermograms are usually related to high emissivity values. The presence of the main low-temperature anomalies can be justified by humid materials (characterized by a higher thermal capacity) and/or t by differences in emissivity and roughness. The time-lapse approach and parametric analysis of temperatures variation can help the interpretation of IRT results.

The PCA highlights different types of thermal response for each specific analyzed areal sector of the surveyed surface. In this respect, Fig. 7 shows some PCA results of dynamic IRT data in terms of the autovectors (blue curve on the right column): along their directions, the dataset is progressively projected with the associated scores for each pixel shown in the panels on the left (eigenvalues).

In Fig. 7, the first (in terms of statistical representativity) three (independent) autovectors are plotted. Qualitatively, they have opposite behaviors:

i) the first principal component describes the mean dynamic during the experiment, with a heating energization followed by the natural cooling phase and the scores image showing how much each pixel responds to this sequence;
ii) the second principal component concerns the mean residual dynamic with respect to the first principal component projection, and has opposite trends, with a cooling phase followed by a heating one;
iii) the third principal component has also a first cooling stage followed by a heating phase, but shows a mean behavior which is no anymore pseudo-linear but rather curved.

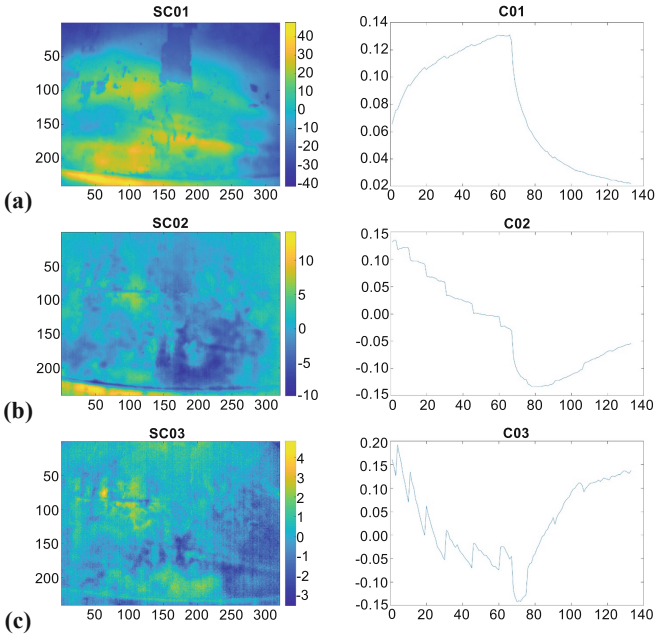

Fig. 7. PCA results of IRT survey for the first acquisition dataset, in terms of eigenvectors (blue curves on the right) and scores matrices (images on le left): first (a), second (b) and third (c) principal component results. (Color figure online)

The first two scores images have ranges of variability evidencing that the first component is one order of magnitude more meaningful in terms of the time-lapse representativity.

Principal components following the third have less variance differences from each preceding one, maintaining a spatial coherence of the scores images up to the sixth principal component, but continuing to show the same order of magnitude as the second one up to, at least, the eighth, substantially being the last two investigated random noise maps.

First component image is strongly influenced by the energization geometries and by properties of the exposed surfaces (e.g. material/emissivity, surface displacement and roughness), while these effects are not so evident in the others. Some radiometric artifacts due to optics are also fully included in the first component image like vignetting effects on the borders of the image.

Further detailed analysis of PCA is extending the interpretation to the first six principal components projections. More in depth analyses are in progress to map in detail the features of the materials and to correlate the thermal behavior of the different homogenous zones to the nature and the origin of the thermal anomalies.

Looking at the time-lapse dataset, PCA can be integrated by the analytical approaches based on data regression. In the cases the regression model can describe and summarize the experimental behavior, outputs maintain a physical meaning of the maps like, for instance, in the case of Intercept Temperature (T_0) and Thermal Gradient (TG or dT/dt) in Fig. 8. The two maps in Fig. 8 are qualitatively very similar but in-depth analysis allow to give significant sparks for the thermal behavior classification of the inspected pixels.

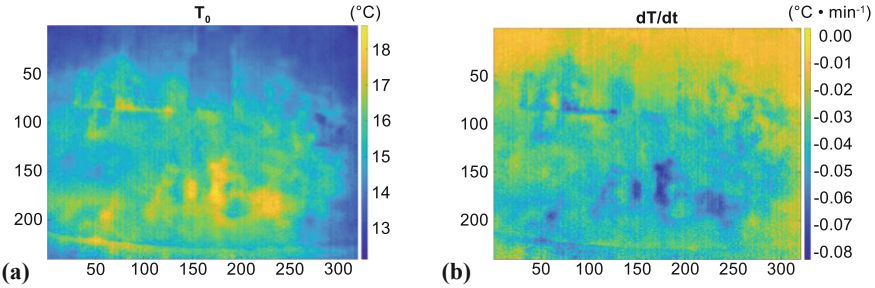

Fig. 8. Results of cooling dataset linear regression: (a) Intercept Temperature (T_0) and (b) Thermal Gradient (dT/dt).

Their joint analysis provides evidences of different behavior of heat flux diffusion towards the inner parts of the wall (Fig. 9). Scatter diagram in Fig. 9.a confirms that T_0 and TG maps are strongly correlated but composite RGB image in Fig. 9.b suggests some interesting features: this map has been produced normalizing T_0 and TG matrices and putting normalized T_0 matrix on red channel, normalized TG matrix on green channel, and a flat 255-value matrix on blue channel. In the composite RGB image,

blue pixels imply that a small thermal dynamic was recorded (small T_0 and TG values) while white regions are indicative of the opposite behavior (high T_0 and TG values).

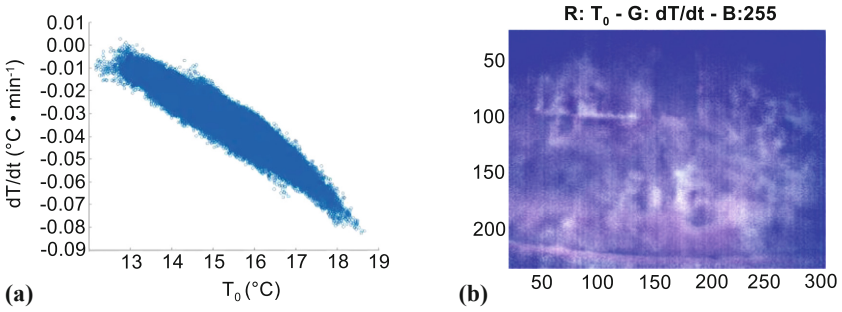

Fig. 9. Results comparison of the correlations between the two thermal indices obtained by the cooling dataset linear regression: (a) Scatter diagram (dT/dt versus T_0) and (b) RGB composite image (R: T_0; G: dT/dt; B: 255). (Color figure online)

Purple-dominating areas, corresponding to high T_0 and common TG values, identify patterns of anomalously high energization due to the geometries of IR lamps emitting lobes: in fact, in these pixels the high temperature reached at the end of the heating phase doesn't correspond to high TG during the cooling phase. Conversely, white patterns are more suspicious of defects such as plaster detachments and air bubbles because to a high temperature reached at the end of the heating phase corresponds a quick cooling stage. Some blue areas correspond to exposed surfaces without the most external plasters, while some others are the signature of the same vignetting feature observed in the scores map related to the first principal component of the full thermal cycle analysis.

3.3 Multispectral Results

Multispectral data were collected across the walls of the most Eastern room of the military complex with controlled and artificial illumination conditions. Inspected surfaces present signs, drawings and paintings over two different materials: wooden tables and plastered walls with paintings outcropping in some areas characterized by missing external finishes. Acquisition points were set at about 1.5 m from the targets.

The multispectral observations made possible to read parts of writings in the wooden tables hidden by dirt and even scraped regions (Fig. 10); so, the longer wavelengths (lambda > 850 nm and >950) of the NIR signals sensed the traces of the inks penetrated the wooden medium. The difference in contrast of the two images is partially due to the narrower band associated to 950 nm high-pass filter acquisition which implies a lower quantity of energy reaching the sensor.

Other EM bands were more effective in evidencing and differentiating elements of varying conditions, such as scrapes or grooves. On the other targets, during the multispectral survey, MIS technique allowed enhancement other writings and a drawing



Fig. 10. Detail of stacked multispectral images focusing on an old writing over a table of the recycled wooden coating of part of the walls: at IR850 and partially at IR950 high pass band, the original writing "DISTRIBUZIONE" (distribution, in Italian) is readable, while it is not, when higher frequencies are used (in particular within the visible frequency range and even worse with UV data).

over the same type of wooden support and some paintings that were realized in an intermediate plaster which was only partially visible because it was somewhere crashed down and otherwhere covered by thick opaque layers of other finishes.

The multispectral imaging was not able to penetrate these most superficial opaque layers but allowed to record different spectral responses of the exposed paintings elements. In particular, a big difference between the historically exposed and some close surfaces was detected for wide extensions: the second surfaces were probably exposed only in recent times, as it was inferable by the features and the borders of their crashed elements. This different response could be due to different moisture conditions and also to different oxidation stage.

4 Conclusion

The complementary use of Ground Penetrating Radar surveys, Infrared Thermography and Multispectral Imaging techniques allowed to define an integrated fully non-invasive diagnostic protocol for historical buildings. The methodological approach was designed to perform a reliable analysis of the integrity status of the materials (internal surfaces and wall paintings) and to inspect underground structures. Two internal environments of an ancient building in the historical centre of Cagliari were explored through a GPR survey. The sectors characterized by significant amplitude of the reflected signals were identified. The origin of the main GPR anomalies was strongly uncertain and suggested future further analyses. Infrared Thermographic survey allowed to map degradation phenomena and shallow stains on the surfaces of the internal walls of the building. Multispectral imaging was utilized to improve the readability of old writings on wooden supports.

Acknowledgements. Authors would like to thank also Luigi Noli and Mario Sitzia from University of Cagliari for their invaluable technical support. This research was performed with the fundamental help of the students of the degree in Architecture. Moreover, this work would not be possible without the support of the in charge local authorities of *Comando Militare Esercito "Sardegna"*. Authors thank all of them for their contribution.

References

1. Cataldo, R., De Donno, A., De Nunzio, G., Leucci, G., Nuzzo, L., Siviero, S.: Integrated methods for analysis of deterioration of cultural heritage: the Crypt of "Cattedrale di Otranto". J. Cult. Heritage **6**(1), 29–38 (2005)
2. Abu-Zeid, N., Botteon, D., Cocco, G., Santarato, G.: Non-invasive characterisation of ancient foundations in Venice using the electrical resistivity imaging technique. NDT&E Int. **39**, 67–75 (2006)
3. Solla, M., Lorenzo, H., Rial, F.I., Novo, A.: Ground-penetrating radar for the structural evaluation of masonry bridges: results and interpretational tools. Constr. Build. Mater. **29**, 458–465 (2012)
4. Trogu, A., Ranieri, G., Calcina, S.V., Piroddi, L.: The ancient Roman aqueduct of Karales (Cagliari, Sardinia, Italy): applicability of geophysics methods to finding the underground remains. Archaeol. Prospect. **21**(3), 157–168 (2014)
5. Casas, A., et al.: Non-invasive geophysical surveys in search of the Roman Temple of Augustus under the Cathedral of Tarragona (Catalonia, Spain): a case study. Surv. Geophys. **39**, 1107–1124 (2018). https://doi.org/10.1007/s10712-018-9470-6
6. Piga, C., Piroddi, L., Pompianu, E., Ranieri, G., Stocco, S., Trogu, A.: Integrated geophysical and aerial sensing methods for archaeology: a case history in the Punic Site of Villamar (Sardinia, Italy). Remote Sens. **6**(11), 10986–11012 (2014)
7. Piroddi, L., Loddo, F., Calcina, S.V., Trogu, A., Cogoni, M., Ranieri, G.: Integrated geophysical survey to reconstruct historical landscape in Undug areas of the Roman ancient town of Nora, Cagliari, Italy. In: 2018 Metrology for Archaeology and Cultural Heritage, pp. 244–248. IEEE, New York (2018)

8. Piroddi, L., Calcina, S.V., Trogu, A., Ranieri, G.: Automated resistivity profiling (ARP) to explore wide archaeological areas: the prehistoric site of Mont'e Prama, Sardinia, Italy. Remote Sens. **12**, 461 (2020). https://doi.org/10.3390/rs12030461
9. Pirinu, A., Balia, R., Piroddi, L., Trogu, A., Utzeri, M., Vignoli, G.: Deepening the knowledge of military architecture in an urban context through digital representations integrated with geophysical surveys. The city walls of Cagliari (Italy). In: 2018 Metrology for Archaeology and Cultural Heritage, pp. 211–215. IEEE, New York (2018)
10. Calcina, S.V., Piroddi, L., Ranieri, G.: Fast dynamic control of damaged historical buildings: a new useful approach for Structural Health Monitoring after an earthquake. ISRN Civil Eng. **2013**, 1–6 (2013)
11. Calcina, S.V., Piroddi, L., Ranieri, G.: Vibration analysis of historic bell towers by means of contact and remote sensing measurements. Nondestr. Test. Eval. **31**(4), 331–359 (2016)
12. Marchisio, M., Piroddi, L., Ranieri, G., Calcina, S.V., Farina, P.: Comparison of natural and artificial forcing to study the dynamic behavior of bell towers in low wind context by means of ground-based radar interferometry: the case of the Leaning Tower in Pisa. J. Geophys. Eng. **11**(5), 055004 (2014)
13. Piroddi, L., Calcina, S.V.: Integrated vibration analysis for historical dome structures: a complementary approach based on conventional geophysical methods and remote sensing techniques. In: Gervasi, O., et al. (eds.) ICCSA 2020. LNCS, vol. 12249–12255, pp. 928–943. Springer, Heidelberg (2020, in press)
14. Calcina, S.V., Piroddi, L., Ranieri, G., Trogu, A.: Terrestrial remote sensing and microtremor measurements for the study of the vibrations of a rock mass with large underground cavities. Rendiconti Online della Società Geologica Italiana **35**(2015), 46–49 (2015). https://doi.org/10.3301/ROL.2015.60
15. Cosentino, P.L., Capizzi, P., Fiandaca, G., Martorana, R., Messina, P.: Advances in microgeophysics for engineering and cultural heritage. J. Earth Sci. **20**(3), 626–639 (2009). https://doi.org/10.1007/s12583-009-0052-x
16. Cosentino, A., Gil, M., Ribeiro, M., Di Mauro, R.: Technical photography for mural paintings: the newly discovered frescoes in Aci Sant'Antonio (Sicily, Italy). Cons. Patrim. **20**, 23–33 (2014)
17. Piroddi, L., Vignoli, G., Trogu, A., Deidda, G.P.: Non-destructive diagnostics of architectonic elements in San Giuseppe Calasanzio's church in Cagliari: a test-case for micro-geophysical methods within the framework of holistic/integrated protocols for artefact knowledge. In: 2018 IEEE International Conference on Metrology for Archaeology and Cultural Heritage, pp. 17–21. IEEE, New York (2018)
18. Ranieri, G., et al.: Method and system for activating and controlling a water-repelling process in walls. European Patent EP3040490B1, priority 2014-12-30, grant 2017
19. Fiorino, D.R., Pirinu, A.: Interdisciplinary contribution to the protection plan of the fortified old town of Cagliari (Italy). Int. J. Heritage Archit. **1**(2), 163–174 (2017)
20. Fiorino, D.R., Santoni, V.: Scenari di riconversione del Bastione di San Filippo a Cagliari. Proposte progettuali per un Distretto dell'Arte (Perspectives for the reconversion of the San Filippo Bastion in Cagliari. New design proposals for an Art District). In: Damiani, G., Fiorino, D.R. (eds.) Military Landscapes, pp. 125–136. Skira, Milan (2017)
21. Fiorino, D.R., Iannotti, P., Mellano, P.: Il riuso delle aree militari in Italia: esperienze di ricerca e didattica per le caserme di Bolzano e Cagliari in Il patrimonio culturale in mutamento. Le sfide dell'uso. In: 35° Convegno Internazionale Scienza e Beni Culturali, pp. 749–760. Edizioni Arcadia Ricerche, Marghera Venezia, Italy (2019)
22. Davis, J.L., Annan, A.P.: Ground-penetrating radar for high-resolution mapping of soil and rock stratigraphy. Geophys. Prospect. **37**, 531–551 (1989)

23. Avdelidis, N.P., Moropoulou, A.: Applications of infrared thermography for the investigation of historic structures. J. Cult. Heritage **5**, 119–127 (2004)
24. Martinetti, S., Grinzato, E., Bison, P.G., Bozzi, E., Cimenti, M.: Statistical analysis of IR thermographic sequences by PCA. Infrared Phys. Technol. **46**, 85–91 (2004)
25. Piroddi, L., Ranieri, G.: Night thermal gradient: a new potential tool for earthquake precursors studies. An application to the seismic area of L'Aquila (central Italy). IEEE J. Sel. Top. Appl. Earth Observ. Remote Sens. **5**(1), 307–312 (2011)
26. Piroddi, L., Ranieri, G., Freund, F., Trogu, A.: Geology, tectonics and topography underlined by L'Aquila earthquake TIR precursors. Geophys. J. Int. **197**(3), 1532–1536 (2014)
27. Piroddi, L.: From high temporal resolution to enhanced radiometric resolution: Night Thermal Gradient results. In: International GeoHazard Research Society (IGRS) 2014 Symposium at NASA Ames Research Center, 10 December 2014, Moffett Field, California, USA (invited speech) (2014)
28. Piroddi, L.: From high temporal resolution to synthetically enhanced radiometric resolution: insights from Night Thermal Gradient results. Eur. Phys. J. Spec. Top. (2020, in press). (Freund, F., Kamer, Y., Ouillon, G., Scoville, J., Sornette, D. (eds.) ISSN: 1951-6355 (Print Edition), ISSN: 1951-6401 (Electronic Edition))
29. Lerma, J.L.: Automatic plotting of architectural facades with multispectral images. J. Surv. Eng. **131**(3), 73–77 (2005)
30. Remondino, F., Rizzi, A.: Reality-based 3D documentation of natural and cultural heritage sites-techniques, problems, and examples. Appl. Geomat. **2**(3), 85–100 (2010)
31. Cogoni, M.: Nuove tecnologie non distruttive per lo studio e il restauro dei beni monumentali: applicazioni termografiche e multispettrali nell'ipogeo di San Salvatore di Sinis in Cabras. Master degree thesis in Conservazione dei beni architettonici e ambientali, academic year 2014/15
32. Piroddi, L., Ranieri, G., Cogoni, M., Trogu, A., Loddo, F.: Time and spectral multiresolution remote sensing for the study of ancient wall drawings at San Salvatore hypogeum, Italy. In: Proceedings of the 22nd European Meeting of Environmental and Engineering Geophysics, Near Surface Geoscience 2016, pp. 1–5. EAGE, Houten (2016)
33. Trogu, A., Cogoni, M., Ranieri, G., Piroddi, L., Loddo, F.: Invisible but not lost. The recovery of the wall drawings of the hypogeum of San Salvatore di Sinis (Sardinia, Italy). In: Proceedings of 24th Annual Meeting of the European Association of Archaeologists, vol. 1, p. 489. Edicions de la Universitat de Barcelona, Barcelona (2018)
34. Piroddi, L., Calcina, S.V., Trogu, A., Vignoli, G.: Towards the definition of a low-cost toolbox for qualitative inspection of painted historical vaults by means of modified DSLR cameras, open source programs and signal processing techniques. In: Gervasi, O., et al. (eds.) ICCSA 2020. LNCS, vol. 12249–12255, pp. 971–991. Springer, Heidelberg (2020, in press)
35. Menezes, A., Glória Gomes, M., Flores-Colen, I.: In-situ assessment of physical performance and degradation analysis of rendering walls. Constr. Build. Mater. **75**, 283–292 (2015)